Experimental characterization of the constitutive materials of an old masonry vaulted tunnel of the Paris subway system

Omar Moreno Regan, Anne Sophie Colas, Emmanuel Bourgeois, Patrice Chatellier, Alain Desbordes, Jean-François Douroux

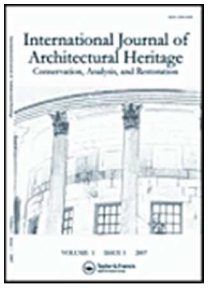

Experimental characterization of the constitutive materials of an old masonry vaulted tunnel of the Paris subway system

Journal:	*International Journal of Architectural Heritage*
Manuscript ID	UARC-2016-1604.R1
Manuscript Type:	Original Article
Date Submitted by the Author:	17-Mar-2017
Complete List of Authors:	Moreno Regan, Omar; Universite Paris-Est Marne-la-Vallee; IFSTTAR Colas, Anne-Sophie ; Universite Paris-Est Marne-la-Vallee; IFSTTAR Bourgeois, Emmanuel; Universite Paris-Est Marne-la-Vallee; IFSTTAR Chatellier , Patrice; Universite Paris-Est Marne-la-Vallee; IFSTTAR Desbordes, Alain; RATP Douroux, Jean-François; RATP
Keywords:	Masonry, Tunnel, Metro, Vault, Experimental characterization, Masonry interface, Millstone, Direct tensile strength, Fracture energy

Experimental characterization of the constitutive materials of an old masonry vaulted tunnel of the Paris subway system

Omar Moreno Regan[1], Anne-Sophie Colas[2], Emmanuel Bourgeois[1], Patrice Chatellier[1]

Alain Desbordes[3], Jean-François Douroux[3]

[1] Université Paris-Est, COSYS, LISIS, IFSTTAR, F-77447 Marne-la-Vallée, France

omarmorenoregan@hotmail.com

emmanuel.bourgeois@ifsttar.fr

patrice.chatellier@ifsttar.fr

[2] Université Paris-Est, MAST, SDOA, IFSTTAR, F-77447 Marne-la-Vallée, France

anne-sophie.colas@ifsttar.fr

[3]RATP

50 Rue Roger Salengro, 94724 Fontenay-sous-bois, France

alain.desbordes@ratp.fr

jean-francois.douroux@ratp.fr

Corresponding author:

Omar Moreno Regan

Université Paris-Est, IFSTTAR

omarmorenoregan@hotmail.com

Abstract

An important part of the Paris metro comprises a masonry vault and unreinforced concrete sidewalls and slab. Masonry consists of stone blocks and mortar joints. In order to evaluate the structural state of an existing tunnel, it is necessary to know the mechanical properties of the materials of which the tunnel is built. Yet, the properties of the materials of the tunnels are rarely thoroughly studied, and some other properties are not at all available. In this perspective, an extensive laboratory test campaign was undertaken to characterize the properties of the materials of the vault and sidewalls. The tested properties include mode I fracture energy, direct tensile and shear strength, as well as the complete tensile characterization of the masonry interface. These tests were carried out on specimens taken from cores extracted *in situ*. This paper presents the results obtained for masonry, individual components, i.e. mortar and stone, and concrete.

Running Head: Experimental tests on old masonry tunnel materials

Keywords: Masonry · Tunnel · Metro · Vault · Experimental characterization · Masonry interface · Millstone · Direct tensile strength · Fracture energy

1. Introduction

The Paris subway system, operated by the Régie Autonome des Transports Parisiens (RATP), has sixteen lines and carries about 5 million passengers daily. The infrastructure is mostly underground and was built predominantly in the early twentieth century. About 85% of the tunnels comprise a masonry vault and unreinforced concrete sidewalls and slab.

The construction of the first line of the Paris subway system started in 1898. The typical section adopted for the tunnels between stations was an elliptic masonry vault built with blocks of millstone and mortar, the masonry of the tunnel vault is arranged following a running bond; the sidewalls and ground slab were slightly curved and made with unreinforced concrete (see Fig. 1). This construction technique was used until late 1950's and still represents the main part of the underground assets of the Paris subway system.

According to (Biette 1928) the block stones used for the masonry of the vault were mostly of millstone or gritstone (Fig. 2), a siliceous stone, considered cellular, sometimes spongy and highly porous, formed of quartz fragments of carbonate of lime, alumina and iron oxide, in various proportions.

According to (Mesnager 1923), given the wide variety of the internal structure of this stone, its compressive strength can range from 2 up to 220 MPa. Description presented by (Biette 1928) reports that the mortar used to join the stone blocks was generally made out of Portland cement or slag cement dosed with 300-350 kg mass of cement per m^3 of sand. Concrete used for the sidewalls and the slab was obtained by mixing 0.8 m^3 of gravel with 0.5 m^3 of mortar, the latter being dosed in the proportion of 400 kg mass of Portland cement per m^3 of sand.

The maintenance and the evaluation of the current state of an existing tunnel is a key priority to the RATP in order to ensure the continuity of the metro service. To evaluate the serviceability state of a tunnel, for instance when nearby civil engineering works are carried out, it is necessary to predict the behavior of the masonry vault and the concrete walls and slab using advanced numerical tools, to assess any possible impact on the existing structure.

In order to perform numerical modeling, the mechanical properties of the materials are need to be known. Yet, little information can be found in the literature regarding the properties of the materials that were used to build these tunnels, and some other parameters are not at all available.

Tests carried out in different masonry structures made of bricks and mortar have been reported in the literature, for instance: (McNary et Abrams 1985), (Binda, Fontana et Frigerio 1988), (Domède, et al. 2009), (Domede, Sellier et Stablon 2013), (Drougkas, Roca et Molins 2016) and (Pelà, P. et Benedetti 2016) tested the compression strength, (Backes 1985) tested the tensile strength parallel to the bed joint, (Vermeltfoort et Raijmakers 1993) tested the shear strength, (Page 1981) and (Dhanasekar, Page et Kleeman 1985) tested the biaxial strength. However, experimental results presented in the literature on masonry structures are conducted mainly in brick masonry, and very limited data is available on stone masonry. Basic mechanical properties of the masonry of the Paris metro stations were tested by (Llanca, et al. 2013) in order to establish a methodology to diagnose the lining status by geoendoscopy, nevertheless the tests carried out in the composite masonry samples do not provide full stress-strain curves including the post-peak part. Some basic strength values for millstones are provided by (Saade, et al. 2013).

In this perspective, tests were carried out on all the materials composing the tunnel to obtain their properties, including parameters that are not commonly studied for these tunnels. Notably, mode I fracture energy, direct tensile and shear strength, as well as the complete tensile characterization of the interface were determined for the first time in this study. Also, experimental correlations between shear and compressive strength, and between mode I fracture energy and tensile strength were obtained. All these parameters, together with the full stress-strain curves including the post-peak part, are needed to perform advanced numerical modelling, see for instance (Berto, et al. 2002), (Creazza, et al. 2002), (Zucchini et Lourenço 2004), among many others. It is stressed that the stone and the mortar of the masonry of the tunnel have never been studied separately.

To perform the experimental tests, 32 cores were extracted from a tunnel in line 3 of the Paris metro to perform an extensive study of the mechanical properties. The objective of the tests is to provide all the necessary parameters to carry out an advanced numerical modeling.

2. Materials and methods

2.1. Extraction of the samples

The materials of a tunnel and a station of the line 3 of the Paris metro, built in the 1930s, were studied. A total of 32 cores were extracted from five positions (Fig. 3a) with a 106 mm diameter core drilling sampler for the sidewalls and a 76 mm diameter for the masonry vault (Fig. 3b). Core extraction was executed following the French standard NF EN 12504-1 (AFNOR April 2012). Drilling was carried out with water to avoid excessive friction and overheating of the core sampler. A description of the extracted raw cores is presented in Table 1.

2.2. Visual inspection

A visual inspection of the specimens showed that the masonry has generally mortar joints ranging from 2.5 cm to 10 cm. The size of the Millstone blocks is highly variable from one core to another, ranging from 5 to 30 cm long, and sometimes occupying the entire length of the core.

The masonry mortar joints contain larger diameter aggregates than modern day mortars. A visual and photographic analysis of the specimens shows that the size of the aggregates varies from 3 to 15 mm, with an average of 7 mm (Fig. 4a). In other words, it would be more accurate to call the joints "concrete joints" rather than "mortar joints". However, to avoid confusion with the concrete of the sidewalls, they will be called "mortar joints" in the following. The concrete of the sidewalls has quite large aggregates. A visual analysis shows that the aggregate size varies from 6 to 58 mm with an average of 25 mm (Fig. 4b). It can be defined as a cyclopean concrete. The average values of the size for the aggregates for the mortar and concrete were determined by measuring them in the surface of 6 and 9 specimens, respectively.

2.3. Preparation of specimens

An important work was carried out to prepare the specimens from the raw cores extracted from the tunnel. The cores were sorted out to identify the samples to be used for testing, and then adjusted to satisfy the dimensions required by the tests standards. However, for some tests these requirements were not met given the fact that the size of the specimens was limited by the size of the mortar

joints/blocks of stone in the masonry cores. The masonry raw cores were sawn and cut out to obtain 50 mm diameter cylindrical specimens of each composing material. Finally, all the prepared test specimens, except those used for shear and density tests, were subjected to a mechanical surfacing, executed with a lapping and polishing machine (Fig. 5a). The flatness of the specimens was then controlled with a flatness gauge (Fig. 5b) to check the tolerances required by the standards.

2.4. *Studied properties*

The properties tested in each material of the tunnel are:

- Bulk density, ρ_d
- Water accessible porosity, p_o
- Compression strength, f_c
- Young's modulus, E
- Poisson's ratio, v
- Direct tensile strength, f_t
- Mode I fracture energy, G_{ft}
- Shear strength, f_s

The determination of these parameters was made according to the standards for each type of material. The objective is to obtain full stress-strain curves for each constitutive material of the tunnel.

The result of each test is presented in the following with its mean value and its coefficient of variation (CV in percentage). Except where indicated otherwise, Chauvenet's criterion was used to discard extreme values.

2.5. *Compression tests*

The compression strength, Young's modulus and Poisson's ratio were obtained following the standards for each material on cylindrical specimens with a slenderness ratio of 2. An extensometer called "J2P" was used to measure the deformations of the specimen. This device is a strain gauge consisting of two rings fixed to the specimen through attachment tips (Fig. 6a) that are pressed into the specimen by screws; the rings are separated of a distance of 70 mm. Three longitudinal LVDT sensors

are fixed vertically positioned at 120° to measure the displacement between the two rings that fallow the deformation of the specimen through the attachments; the sensor is fixed on the upper ring with a screw whereas the lower ring provides a plane surface of reference (Fig. 6b). Three transverse LVDT sensors are also disposed at 120° fixed with a screw and in contact with the specimen to measure the transverse deformations at the bottom (Fig. 6b). This method of measuring was proposed by (Boulay et Colson 1981). Full strain-stress curves are obtained by controlling the displacement of the hydraulic jack, which allows obtaining the reduction of the stress after the peak has been exceeded. A ratio in µm/s is given to the computer that controls the loading device. These ratios, standards and specimens' dimensions are specified for each material in the following sections.

2.6. Direct tensile tests

The procedure for the direct tensile test is the same as that used by (Rossi, et al. 1994) for quasi-static tensile test in concrete. The tests were carried out on cylindrical specimens with a slenderness ratio of 2. The procedure is as follows: the ends of the cylindrical specimen are glued to two aluminum caps, which have the same diameter as the specimens, that are attached to the loading device (by screws); the lower hydraulic jack of the loading device moves vertically downward, thereby exerting a direct tensile force on the specimen (see Fig. 7a). Three pairs of supports arranged at 120° are glued to the specimen (see Fig. 7b) to receive the three LVDT displacement sensors. These supports are made of metallic rectangular prisms of about 20 mm per side with a circular hole that allows to receive the sensor; one of its external faces have a toothed surface on which glue is applied for a better adhesion to the specimen. The supports are separated vertically of about 55 mm and 170 mm for the 50 mm and 104 mm diameter specimens, respectively. The sensor is fixed in the upper support with a screw, whereas the lower support provides a plane surface of reference, thus the displacement measurement is carried out between the two glued supports. Three additional sensors are attached to the aluminum caps, to measure the overall elongation of the specimen. Before starting the tensile test, a pre-compression load of 3 and 5 kN is applied for the 50 mm and 104 mm diameter specimens, respectively, for about 30 min, the time required for the glue to set. The tensile load is applied

controlling the displacement of the hydraulic jack by imposing a ratio in µm/s to the load device. Ratios and specimens' dimensions are specified for each material in the following sections.

The glue used is a composite distributed by Brenntag, consisting of Plex 7742-F powder and Pleximon 801 liquid, dosed at 8 ml of liquid for 37.5 g of powder, which provides a pull-out resistance of about 30 MPa for standard concrete.

The direct tension tests and the fictitious crack approach proposed by (Hillerborg, Modéer et Petersson 1976) were chosen to calculate the mode I facture energy. In this model, the area under the curve stress-crack opening (σ-w) represents the fracture energy by unit area of the fracture surface, defined as the projected area in a plane perpendicular to the direction of the stress. The fracture energy G_{ft} is calculated from the equation:

$$G_{ft} = \int_0^{w\max} \sigma(w)dw \quad (1)$$

where w_{max} represents the maximum crack opening. Given the fact that this energy is measured by unit area, the measuring units are N/m or Pa.m.

The crack opening w is computed after the maximum tensile stress has been reached by removing the elastic strain from the measured displacement:

$$w = \Delta l_0 - \frac{\sigma}{E_t} l_0 \quad (2)$$

where Δl_0 is the mean longitudinal displacement of the three sensors, l_0 the distance between the two supports of the LVDT sensors and σ the tensile stress. The tensile Young's modulus E_t was estimated for each specimen with the formula:

$$E_t = \frac{\Delta\sigma}{\Delta\varepsilon} = \frac{\sigma_{30} - \sigma_5}{\varepsilon_{30} - \varepsilon_5} \quad (3)$$

where the subscripts 5 and 30 indicate the values at 5% and 30% of the maximum value of the tensile stress. These values were proposed based on the estimation of the elastic modulus in compression: for concrete (AFNOR february 2014) it is demanded the values at 10% and 33% of the compression strength and for the natural stone (AFNOR august 2005) 2% and 33%. This modulus was estimated with a monotonic loading.

2.7. Shear tests

The shear test is inspired from the Japanese standard (JSCE 1983)-G 553 and was developed specially for this study. This approach has been used in particular by (Mirsayah et Banthia 2002) for fiber concrete on rectangular prisms. In our study, these prisms were replaced by cylinders, given the shape of the extracted cores.

The tests are carried out in cylindrical specimens of 73 mm dimeter and 101 mm height for mortar and stone, and 104 x 201 mm for concrete. The specimen is subjected to a double shear applied at the right of two notches, previously created in the cylinder with a saw, of 12-13 mm depth and 2 mm wide for mortar and stone, and 17 x 6 mm for concrete. To apply the shear force, the ends of the specimen are placed on two semicircular supports and subjected to a vertical force exerted by the loading device on two other semicircular supports placed in the central part (see Fig. 8). These force-transmitting supports are fixed with screws to a metallic plate. For the 73 and 104 mm diameter specimens, the distance between inner walls of the lower supports is 58 and 115 mm, the distance between outer walls of the upper (central) supports is 52 and 102 mm, respectively.

Neoprene plates were placed between the support and the specimen to ensure a uniform contact.

The shear strength τ_{max} is calculated from:

$$\tau_{max} = \frac{P_{max}}{2\pi r^2} \quad (4)$$

where P_{max} is the failure load and r is the radius of the notched section. To measure the deformations of the specimen, supports were glued on both sides of notches in order to receive the LVDT sensors that measure the sliding and opening of the notch, as showed in Fig. 8. The characteristics of these sensor supports are the same as those used in the direct tensile tests (section 2.6)

3. Results and discussion

3.1. Mortar

To isolate the mortar from the masonry raw cores, mortar specimens were sawed and cored from the 73 mm diameter cores taken *in situ*, to obtain 50 mm diameter mortar samples with slenderness ratio

of 2 (Fig. 9), except for the density, porosity and shear tests, where the slenderness ratio was irrelevant, we used 73 mm diameter specimens. It should be noticed that, consequently, it was not always possible to comply with the dimensions imposed by the standards for testing.

3.1.1. Density and porosity

Testing of porosity accessible to water and bulk density were carried out according to the French standard NF P 18-459 (AFNOR march 2010) on nine specimens of average 73 mm diameter and 55 mm height. The minimum volume (0.4 liters) for the specimen imposed by the standard could not be met because of the size of the available raw masonry cores. Specimens showed an average difference of -40% compared to the standard. Results are presented in Table 2; the mean bulk density of mortar is 2010 kg/m^3 with 24% porosity.

3.1.2. Young's modulus

The tests for Young's modulus were performed on five specimens of 50 mm diameter and 98 mm height with a cyclic loading. Four of these were conducted up to failure in compression. The characteristics of the prepared samples taken from the masonry cores were compared with the tolerances required by the French standard NF EN 12390-1 (AFNOR november 2012). The minimum diameter of 100 mm could not be met because the size of the specimens was limited by the size of the mortar joints in the masonry. The test was performed according to the French standard NF EN 12390-13 (AFNOR february 2014).

See Table 2 for the results. The mean Young's modulus of mortar is 19.4 GPa with a Poisson's ratio of 0.15. Although this value is expected for this type of material, it is lower than the corresponding elastic modulus derived from its mean compressive strength given by the Eurocode 2 (AFNOR october 2005) for concrete:

$$E_{cm} = 22\left(\frac{f_{cm}}{10}\right)^{0.3} = 29\ \text{GPa} \quad (5)$$

where f_{cm} =25,5 MPa is the mean compressive strength (see Table 2).

3.1.3. Compressive strength

Compression tests were performed on ten specimens of 50 mm diameter and 97 mm height. The test was performed following the recommendations of the French standard NF EN 12390-3 (AFNOR april 2012), with the exception that the test was displacement controlled, with a 1 µm/s speed, in order to obtain full stress-strain curves. The longitudinal deformations of the specimen were measured using the device described in 2.5. The peak values and the shape of the stress-strain curves show a relatively high dispersion of the results. Fig. 10 shows the expected after-peak softening behavior of the mortar specimens. Results are showed in Table 2; one of the discarded specimens (see section 2.4) was rejected due to improper rupture mode described by the standard. The mean compressive strength is 25.5 MPa.

3.1.4.Direct tensile strength

Twelve specimens of 50 mm diameter and 98 mm height were tested in direct tensile force following the procedure described in 2.6; nine tests were controlled in displacement at a ratio of 0.3 µm/s

The average value of tensile strength of the retained mortar specimens (see section 2.4) is 0.81 MPa, with a considerable dispersion of the results (see Table 2). The stress-strain curves are shown in Fig. 11 for the specimens for which the tests could be satisfactorily carried out. Crack formation was observed in the middle of the specimen.

The mode I fracture energy G_{ft} is obtained with equation (1) and from the calculation of the area under the curve σ-w, obtained from the stress-strain curves (Fig. 11) and equation (2). Using equation (3) for each specimen, an average tensile Young's modulus for the mortar of 9.4 GPa was calculated, versus 19.4 GPa for the compressive modulus obtained experimentally. Considerable dispersion was also observed in the G_{ft} values (see Table 2) when estimating the mean value of 75 Pa.m.

The Pearson correlation coefficient between tensile strength f_t and G_{ft} of the retained mortar specimens is r=0.86. From the experimental results, an original correlation was proposed between these two properties (see Fig. 13):

$$G_{ft} = 100 f_t^{0.8} \quad (6)$$

where f_t is expressed in MPa and G_{ft} in Pa.m; the standard error of the estimate is 25.8 Pa.m. Other correlations between these two properties are proposed in the literature for concrete, for instance the empiric formula proposed by (Bazant et Oh 1983) which also includes the elastic modulus in compression E_c and the aggregate size d_a. This formula would produce however very low values of G_{ft} with respect to the values we found:

$$G_{ft} = \left(2.72 + 3.104 f_t\right) f_t^2 \frac{d_a}{E_c} = 10 \text{ Pa.m} \quad (7)$$

with f_t=1,35 N/mm², E_c=19 400 N/mm² and d_a =14,7 mm. The values of G_{ft} for concrete reported by (A. Hillerborg 1985), ranging from 65 to 200 Pa.m, are more in agreement with the order of magnitude that we found, nevertheless, no correlation between f_t and G_{ft} is provided. A full review on the experimental approaches to estimate G_{ft} in concrete can be found in (Shah, Swartz et Ouyang 1995).

3.1.5. Shear strength

The shear tests were performed on six specimens of 73 mm diameter and 101 mm height, with a 13 mm depth notch, producing a shearing area of approximately 1750 mm², following the procedure described in 2.7. To prevent bending failure mode, three metallic bars of 50 mm long and thickness of 2 mm were glued in the central part of the specimen. When the specimen was mounted in the loading device, these bars were facing down, where the bending is expected.

However, this procedure did not permit to observe a pure shear failure: the initiation of the crack is produced in the lower part of the notch by the shear force, but the crack then propagates by bending (see Fig. 12), because of a rotation of the specimen after the crack initiation. The forces, to which the specimen is subjected under the conditions of this test, are shear at the right of the notch, combined with bending at the center of the specimen.

The obtained data shows a drop of the applied force after the peak at the time of initiation of the crack, followed by an increase of the force corresponding to the bending phase at the end of the test. Correct pure shear full stress-strain curves could not be obtained.

Nevertheless, it is assumed that the maximum load P_{max} corresponds to the pure shear strength. The maximum stress is calculated from the equation (4). The mean value from the four retained specimens (see Table 2) is 1.4 MPa.

Given the mixed mode of failure, mode II fracture energy could not be determined experimentally. Nevertheless, using the shear fracture model for concrete proposed by (Bazant et Pfeiffer 1986b) it is possible to estimate the mode II fracture energy:

$$G_{fs} = \frac{g}{AE_c} f_t^2 d_a \quad (8)$$

where parameters g=2.93 and A=0.00986 are proposed by (Bazant et Pfeiffer 1986b) for the model. The other parameters were obtained experimentally in this study: E_c is the mean elastic modulus of 19 400 N/mm², f_t is the mean direct tensile strength of 0.81 N/mm² and d_a the maximum aggregate size, taken equal to 14.7 mm. The calculated mode II fracture energy of mortar is 148 Pa.m. However, this value is only 2 times higher than the mode I fracture energy, whereas (Bazant et Pfeiffer 1986b) found a ratio of 25 between these two energies for concrete.

Using the mean experimental results, a linear relation between shear strength f_s and compressive strength f_c for mortar can be deduced:

$$f_s = 0.056 f_c \quad (9)$$

3.2. Millstone

The stone specimens were obtained from sawing and coring of the 73 mm diameter raw masonry cores.

3.2.1. Classification of the stone specimens

As mentioned earlier, the composition of the stone used in the construction of the Paris metro is very diverse (Fig. 14). This variety can lead to a wide dispersion of mechanical characteristics and make the average values unrepresentative. It was therefore decided, after a comprehensive analysis of all the mechanical tests, to classify the stone into three categories. The proposed classification searches to provide properties of each category of the stone with a maximum coefficient of variation of about 30%.

As it is seen in the results presented in the following sections, this was achieved for most cases. On the one hand, three limits are proposed regarding the porosity p_0 of the stone (Fig. 14):

- High quality (HQ): $0\% < p_0 \leq 13\%$
- Average quality (AQ): $13\% < p_0 \leq 35\%$
- Low quality (LQ): $p_0 > 35\%$

On the other hand, three limits are proposed for the mechanical property in question, defined by the nearest intersection of the estimation curve and the porosity limits; the estimation curve was obtained for each case by exponential regression. These limits provide the range of values proposed in our study for each category and property; experimental data obtained outside this range was discarded (see Fig. 15). The estimation curve is given by the equation:

$$M = A\exp(Bp_0) \tag{10}$$

where coefficients A et B are given in the following sections for each mechanical property M.

3.2.2. Density and porosity

Testing of porosity accessible to water and bulk density were carried out according to the French standard NF EN 1936 (AFNOR may 2007) on twenty-nine specimens, fifteen with a diameter of 50 mm and fourteen of 73 mm; height varied from 15 to 40 mm. The minimum surface-volume ratio requested by the standard (0.08 mm^{-1}) could not be met given the available size of the specimens, which showed an average difference of -50% compared to the standard. According to the proposed classification (see section 3.2.1), the average values for each category of stone are presented in Table 3. Mean value of the density of the AQ stone is 2060 kg/m^3 with 20% porosity.

Pearson correlation coefficient between porosity and density is r=-0.99. From the experimental results, using linear regression a correlation between these properties was established (see Fig. 16):

$$p_0 = (0.9331 - 0.00035 m_v) \tag{11}$$

where m_v is the bulk density in kg/m^3; the standard error of the estimate is 1.7 %. This relationship was used to estimate the porosity of all the specimens from their bulk density in the rest of the experimental campaign to sort them out based on their porosity.

3.2.3. Young's modulus

Young's modulus tests of the stone were carried out with a cyclic loading according to the French standard NF EN 14580 (AFNOR august 2005) using the extensometer described in 2.5. The campaign covers ten specimens of 50 mm diameter and 97 mm height. Porosity of each specimen was determined with equation (11).

Following the classification proposed in section 3.2.1, results for each type of stone are presented in Table 3, the Poisson's ratio for the low quality stone could not be determined, given the high porosity of the specimen. The AQ stone presents an elastic modulus E_c of 40.5 GPa and a Poisson's ratio of 0.32. Tests carried out on millstone by (Saade, et al. 2013) report much lower values for the elastic modulus, of about 2.5 GPa, with respect to the values found in this study. The difference can be due to the volume of cavities of the millstone specimens used by (Saade, et al. 2013).

Fig. 17 shows the relation between the estimated porosity and Young's modulus, which has a correlation coefficient of r=-0.91. The coefficients of the estimation curve [Eq. (10)] are also showed in Fig. 17; the standard error of the estimate is 6.57 GPa.

3.2.4.Compressive strength

The compression tests were performed according to the French standard NF EN 1926 (AFNOR april 2007). The campaign covers thirteen samples of 73 mm diameter and 70 mm height and thirteen specimens of 50 mm diameter and 96 mm height. Given the height of the 73 mm specimens, it was not possible to use the measuring device described in 2.5, which requires a minimal height of 90 mm for the attachment tips to clamp the specimen properly. These specimens were thus tested only for the maximum force at a rate of 0.5 MPa/s. Fragile and violent failure was found for some specimens, which had very low porosity.

In order to obtain full stress-strain curves, complementary compression tests were performed on thirteen 50 mm diameter specimens. The slenderness ratio 1.0 requested by the standard could not be met for these specimens, which had a 2.0 slenderness ratio. With these specimens the measuring

device for the deformations described in 2.5 was used. The tests were controlled in displacement at a ratio of 0.5 µm/s.

As for the 73 mm samples, low porosity specimens show brittle fracture. Therefore, the full stress-strain curves could not be obtained for all specimens, Fig. 18 a) shows the curves that could obtained.

Following to the proposed classification (section 3.2.1) the results are presented in Table 3. For the 73 mm diameter specimens, the AQ stone present a mean compressive strength of 75.3 MPa.

The porosity of each sample was estimated using the equation (11). In Fig. 18 b) and c) the relation between porosity and compressive strength is showed for each category of stone; one specimen was discarded (see section 3.2.1). The correlation coefficient between these two properties is r=-0.77 and -0.83, for the 50 and 73 mm diameter specimens, respectively; Eq. (10) was also used for the estimation curve, the standard error been 22.6 et 32.5 MPa, respectively.

In general we observe that 73 mm specimens have a higher compressive strength. Using Eq. (10), with its respective A and B values (Fig. 18), for the same porosity, 73 mm specimens produces a higher compressive strength by an average factor of 1.5 with respect to the 50 mm specimens. This can be due to fact that the cavities, present in same size and volume in both type of specimens, tend to produce failure earlier in the 50 mm specimens; and also to the fact that 50 mm specimens have a slenderness ratio of 2, whereas 73 mm specimens have a ratio of 1.

3.2.5. Tensile strength

Direct tensile tests were performed in twelve specimens of 50 mm diameter and 95 mm height according to the procedure described in 2.6. The tests were controlled in displacement at different rates, depending on the composition of the stone, ranging from 0.1 to 0.5 µm/s.

The almost instantaneous and brittle rupture of the most resistant specimens observed in the compression tests was also observed in the tensile tests. This trend can be seen on the stress-strain curves in Fig. 19 a). The specimens with a higher porosity have a softening behavior after the peak. Using equation (11), porosity of each sample was estimated in order to classify the obtained results in function of the porosity limits (section 3.2.1). Table 3 presents the results, the mean tensile strength for

the AQ stone is 3.44 MPa with a mode I fracture energy of 121 Pa.m, using equation (2) to calculate the crack width *w* when possible. For the average and low quality samples, it was possible to obtain the post-peak curve, whereas a fragile facture was observed for high quality stones (Fig. 19 a). This explains the higher values of this energy for the average and low quality compared with high quality stone (see Table 3).

Initial stiffness values for the stone were lower in the tensile tests than those in compression. These were estimated using formula (3) for each specimen, the average values and corresponding CV are:

- High quality (3/12): 49.5 GPa, 24%
- Average quality (4/12): 18.4 GPa, 31%
- Low quality (2/12): 3.1 GPa, 38%

Fig. 19 b) plots the relation between calculated porosity and tensile strength; two specimens were discarded (see section 3.2.1). The correlation coefficient between these two properties is r=-0.88 and the standard error of the estimate [Eq. (10)] is 1.24 MPa.

3.2.6.Shear strength

The shear tests were performed on six specimens of 73 mm diameter and 102 mm height, with a 12 mm depth notch, according to the procedure outlined in 2.7. As for the mortar, metal bars were glued to prevent rupture in the middle of the specimen.

Rupture occurred in shear at the right of the notch, but the crack propagation was produced by bending due to the rotation on the specimen. The observed fracture was brittle in all cases, thereby slipping could not be measured and the mode II fracture energy could not be determined. Nevertheless, we assume that the maximum load corresponds to the pure shear strength of the stone. The estimation of the porosity of each sample with the equation (11) showed that all the selected specimens had an average quality. Results are presented in Table 3; the average value of the shear strength is 4.83 MPa.

From the mean experimental results, a linear relation can be established between the shear strength of an average quality stone and its compressive strength:

$$f_s = 0.064 f_c \quad (12)$$

3.3. Masonry properties

The tests on the stone-mortar composite samples taken from the masonry cores were carried out as complementary tests, to provide orders of magnitude of the different parameters and observe the behavior of the masonry, when tested as a composite.

3.3.1. Density and porosity

As there is no specific standard for testing porosity accessible to water and bulk density in masonry, the tests were performed according to the French standard for stone NF EN 1936 (AFNOR may 2007). A total of eight specimens were tested, six with a diameter of 50 mm and two of 73 mm; height varied from 28 to 79 mm. The minimum surface-volume ratio requested by the standard (0.08 mm^{-1}) could not be met given the size of the available specimens.

Table 4 presents the obtained results; the mean bulk density of the eight specimens is 2030 kg/m^3 with a porosity of 22%. However, this is only an indicative value, since these values depend greatly on the amount of mortar and stone in the sample and the type of stone (see section 3.2).

3.3.2. Young's modulus and compressive strength

The compression tests and Young's modulus of the composite were performed on five cylindrical specimens of 73 mm diameter and 138 mm height with a cyclic loading. The device for measuring the deformation is outlined in 2.5. The Young's modulus was determined according to the French standard for stone NF EN 14580 (AFNOR august 2005).

As expected, results show high dispersion, since the type of stone, the quantity of mortar in the specimen and the interface orientation impacts its behavior. The average Young's modulus is 28.4 GPa (see Table 4). Similar modulus values were reported by (Llanca, et al. 2013) for the masonry of a tunnel of the Paris metro.

In order to measure simple compression on masonry according to the French standard NF EN 1052-1 (AFNOR october 1999), the test has to be performed on a masonry wall. As it was not possible to

build a wall from the extracted materials *in situ*, the standard NF EN 1926 (AFNOR april 2007) for stone was adopted instead. The results show high dispersion (see Table 4), as it might be expected given the disparities in the amount of mortar in the specimens, the orientation of the interface and the quality of the stone.

The rupture occurred mostly in the stone-mortar interface, followed by the crash of mortar and stone. At the end of each test, the mortar portion of each specimen was estimated. In general, we observed that the resistance decreases with the increasing part of mortar, but the low number of tests performed does not allow to obtain a conclusive trend. The average value of the compressive strength for the masonry is 21,7 MPa (see Table 4).

Despite the dispersion of the experimental results when calculating the mean values, we found a good correlation coefficient between the masonry's compressive strength and the Young's modulus of r=0.98, consequently an approximate correlation relationship between these properties is proposed:

$$E_m = 14\left[\frac{f_c}{10}\right]^{0.9} \tag{13}$$

with f_c in MPa and E_m in GPa; the standard error of the estimate is 4.52 GPa. Another approximate formula for estimating the elastic modulus in masonry is proposed by Eurocode 6 (AFNOR March 2013):

$$E_m = K_E f_k \tag{14}$$

with K_E=1000 and f_k the characteristic compressive strength of the masonry. If we use f_k = 21.7 MPa, equation (14) gives 21.7 GPa; whereas the proposed formula in our study, Eq. (13), gives 28.2 GPa for the same compressive strength. The two predicted modulus have a reasonable agreement, but Eq. (13) is closer to the mean value found experimentally.

Eurocode 6 (AFNOR March 2013) also gives a formula to estimate the compressive strength of masonry f_k from the properties of mortar and block (bricks or stone):

$$f_k = K f_b^{\alpha} f_m^{\beta} \tag{15}$$

with f_b and f_m the mean values of the compressive strength of the block and mortar, respectively; K is a coefficient depending on the type of mortar and block, and α=0.7 and β=0.3 are constants. Using (15) with f_b=75.3 MPa (average quality stone, section 3.2.4) and f_m=25.5 MPa (section 3.1.3) and K=0.45 (natural stone and normal use mortar) we find f_k=24.5 MPa, which is close to the mean experimental value.

3.3.3. Tensile strength of the interface

Specimens presenting an approximately horizontal interface were selected. This criterion led us to produce small samples, which were sawed and cut out from the raw masonry cores (Fig. 24 a). The tests were carried out on thirteen specimens of 50 mm diameter and 50 mm high. Procedure for the tests is outlined in 2.6.

The distance between the LVDT supports was 3 cm (see section 2.6). The tests were controlled in displacement on eight specimens at a rate of 0.1 µm/s in order to obtain the complete force-displacement curve. For the remaining five, only the tensile strength was tested. In all cases, the crack occurred in the interface (Fig. 24 b).

Mean values were calculated after eliminating extreme values (see section 2.4). From eleven specimens, the tensile strength mean value of 0.15 MPa with a high CV of 56% (see Table 4). However, according to (Lourenço, Rots et van der Pluijm 1999) typical CV of the tensile strength of the masonry bond ranges between 50% and 80%.

Mode I fracture energy G_{ft} of the interface was also determined from the σ-w curves using equations (1), (2) and (3). The average value found on six specimens is 8.30 Pa.m (see Table 4). An average tensile elastic modulus of 1.96 GPa was observed for the interface.

This test also allowed us to determine the normal stiffness k_n of the masonry interface, which is estimated from the stress-displacement curve σ-u (Fig. 25) and the formula:

$$k_n = \frac{\Delta\sigma}{\Delta u} = \frac{\sigma_{30} - \sigma_5}{u_{30} - u_5} \qquad (16)$$

where the subscripts 5 and 30 indicate the values at 5% and 30% of the maximum value of the tensile test. These values were proposed the same way as for the elastic modulus in tension (see section 2.6). Mean value for the normal stiffness is 64.8 GPa/m; Table 4 show the obtained results. There is again a high dispersion of results (see Table 4), nevertheless, these tests allow us to have an order of magnitude for these quantities obtained experimentally; a higher number of tests would be needed to obtain more accurate properties.

The cohesion between the stone and mortar may depend on the surface condition of the stone or on the size of the specimens. It was observed that the tensile strength is lower in the interface than in the mortar. This is confirmed by observations made during the handling of the raw masonry cores, where the stone was sometimes separated from the mortar, when sawing or coring. The interface is the weakest link of the masonry when it is subjected to a direct tensile stress.

3.4. Concrete properties

The concrete testing was conducted on test specimens of 104 mm diameter and 200 mm height (Fig. 20), except for the determination of the bulk density. The size of the aggregates varies between 6 and 58 mm, with an average of 25 mm. This average value is retained for normative checks.

3.4.1. Density and porosity

Testing of porosity accessible to water and bulk density were carried out according to the French standard (AFNOR march 2010) on six specimens of 104 mm diameter and 142 mm height. All the requirements imposed by the standard were met. Results are presented in Table 5; the mean bulk density of concrete is 2160 kg/m^3 with 18% porosity, one specimen was discarded (see section 2.4).

3.4.2. Young's modulus

Young's modulus tests were carried out with a cyclic loading on seven specimens of 104 mm diameter and 197 mm height, according to French standards NF EN 12390-13 AFNOR (2014) and NF EN 12390-1 AFNOR (2012a).

Table 5 gives the obtained the experimental results. Average elastic modulus is 21.9 GPa with a Poisson's ratio of 0.21. Although a low modulus for structural concrete, by means of formula (5) we find a similar value, around 25 GPa, using the mean compressive strength (see section 3.4.3).

3.4.3. Compressive strength

Compressive tests were performed on a total of seven specimens, the same used for the determination of Young's modulus, following the recommendations of the French standard (AFNOR april 2012), but tests were controlled in displacement at a rate of 1.0 µm/s to obtain the complete stress-strain curves (see Fig. 21). After discarding one specimen (see section 2.4) we found that the mean compressive strength is 16.0 MPa; detailed results are showed in Table 5. It can be noticed that the compressive strength of concrete is smaller than the mortar of the masonry; this can be explained in part by the size of the aggregates in concrete.

3.4.4. Tensile strength

Direct tensile tests were performed on eight samples of 104 mm diameter and 199 mm height. They were carried out following the procedure outlined in 2.6. The tests, controlled in displacement at a rate of 0.1 µm/s, made it possible to obtain full stress-strain curves (Fig. 22).

One extreme value was excluded for the calculation of the average (see section 2.4). Table 5 shows the obtained results; the average tensile strength is 0.48 MPa. Once again we found that the tensile strength of concrete is smaller than that of the mortar of the masonry.

In all tested specimens, the crack developed in the middle, mostly in the paste-aggregate interface. The crack width w was estimated with equation (2) and the tensile modules for each specimen with equation (3). As in the mortar, the experimental results tend to show that the initial stiffness of the concrete is not the same in tension and compression. The average value of tensile module is 5.2 GPa versus 21.9 GPa in compression. Mode I fracture energy was obtained from the σ-w curves and equation (1); the average value is 104 Pa.m (see Table 5).

It was found that the Pearson correlation coefficient between mode I fracture energy and the direct tensile strength of concrete is r=0.42, which is not as high as other correlations found in this study,

nevertheless, a correlation between these two properties is proposed based on experimental results (see Fig. 23):

$$G_{ft} = 150 f_t^{0.5} \quad (17)$$

where f_t is expressed in MPa and G_{ft} in Pa.m; the standard error of the estimate is 25.3 Pa.m. As for the mortar, empiric formula (7) would produce very low values of G_{ft} with respect to the order of magnitude that we found; values reported by (A. Hillerborg 1985) are more in agreement to ours.

3.4.5. Shear strength

Shear tests on concrete were carried out on seven specimens of 104 mm diameter and 201 mm height, with a 17 mm depth and 6 mm thick notch, producing a shearing area of 3800 mm^2 following the procedure presented in paragraph 2.7.

As for the mortar, this device did not allowed to obtain a pure shear failure: the crack initiation is produced by shear at the notched section, but then propagates as depicted in Fig. 12. The rotation of the specimens during the test did not allow the correct measurement of the deformation.

However, it is assumed that the maximum load corresponds to the pure shear strength, when the rupture occurred at the right of the notch. The mode II fracture energy could not be determined given the incorrect failure mode. After discarding one specimen (see section 2.4), using equation (4) on six specimens a mean shear strength of 0.89 MPa was found (see Table 5).

From the average experimental results, a correlation between the shear strength and compressive strength of concrete can be deduced:

$$f_s = 0.053 f_c \quad (18)$$

4. Numerical model

This section presents elements regarding the numerical modeling of the masonry tunnels of the Paris metro. Details of the developed model are given in (Moreno Regan, et al. 2017) and (O. Moreno Regan 2016).

The masonry is modeled as a homogenized continuum media with a nonlinear constitutive law using the finite element method. An analytical engineering approach for the masonry homogenization is adapted to model the tunnel vault. Elastic properties for both stone and mortar are used to determine the orthotropic elastic behavior of the masonry. The nonlinear phase is modelled using a damage law for each component of the masonry. i.e. stone and mortar. To model the nonlinear law, strain-stress curves, including the post-peak part, are used to calibrate the necessary parameters. Mode I fracture energy is used in the regularization technique in tension, to avoid mesh sensitivity problems in the finite element modeling of the damage law. Concrete of the sidewalls is modelled using the same damage constitutive law.

The properties of the masonry interface are particularly useful when modelling the masonry as a discontinuous media, i.e. the masonry is modelled as an assemblage the discrete blocks, joints are viewed as interfaces between the blocks. This modelling approach was used for masonry tunnels by (Idris, Verdel.T et Al-Heib 2008) and (Chen, Yu et Smith 2016), among others.

5. Conclusions

An experimental campaign was carried out to study the mechanical properties of the materials of an old tunnel of the Paris metro, built with a masonry vault and concrete sidewalls. The campaign covers 164 samples obtained from cores extracted *in situ*. Full stress-strain curves, including the post-peak part, were obtained in compression and tension as well as the mode I fracture energy. The masonry of the vault is composed of millstone blocks and mortar joints; tests were carried out on individual components as well as composite ones.

The mortar of the joints, who can be up to 10 cm thick, have a compressive strength common for this type of material but less stiff, when compared to the elastic modulus proposed by Eurocode 2. The fact that the mortar joints have considerable thickness means that the masonry would have a more flexible global behavior. It was also found that mortar is 2 times stiffer in compression than in tension. Concerning the blocks of stone, we found that the millstone has a varied composition, with very different porosities. Consequently, the relations between porosity and the mechanical properties were studied; the stone was then sorted out into three groups accordingly. Porosity can range from 2% to 50%

and mechanical properties can be up to 25 times higher for the lowest porosity specimens, who showed brittle behavior in compression and tension. We observed that most of the specimens belonged to the average quality stone , we thus consider that the properties of this group would be representative of the millstone when performing calculations on these masonry vaults.

High dispersion in the compressive and elastic modulus tests in the composite was found, in part because the quality of the stone and the quantity of mortar play an important role on the results. The interface of the masonry presents low strength and stiffness in tension, inferior than the tensile strength of the mortar of the masonry, making it vulnerable to the creation cracks if stress state is the tunnel vault is altered by an increasing load in the surface.

The mechanical properties of the concrete from the sidewalls presents low strengths and stiffness. Although less porous than the mortar of the masonry, is less resistant, in part because it is made from a mix with large size aggregates. We also observed that the material is stiffer in compression than in tension by a factor of 4.

Finally, from the experimental results, some correlation relationships are proposed to determine the shear strength depending on the compressive strength, and mode I fracture energy from the tensile strength for the mortar and concrete. The latter, is particularly useful when the post-peak part of the strain-stress curves from a direct tensile test is not available.

The obtained results provide the necessary parameters to carry out advanced numerical modeling for this type of old underground structures and to calibrate nonlinear numerical models.

Acknowledgements

This test campaign was performed in the PhD thesis of the first author (O. Moreno Regan 2016), that was developed in the framework of the CIFRE convention 2012-1605 between IFSTTAR, and the administrator of the Paris metro, RATP.

Our thanks are due to Sandrine Ramanich, Franck Guirado, Florent Baby, Renaud-Pierre Martin and François Martineau for their scientific and technical support during the tests.

References

AFNOR. *Concrete. Testing hardened concrete. Testing porosity and density.* NF P18-459. Saint-Denis, France: AFNOR, march 2010.

AFNOR. *Eurocode 2: Design of concrete structures - Part 1-1: general rules and rules for buildings.* NF EN 1992-1-1 . Saint-Denis, France: AFNOR, october 2005.

AFNOR. *Eurocode 6: Design of masonry structures - Part 1-1 : General rules for reinforced and unreinforced masonry structures.* NF EN 1996-1-1 . Saint-Denis, France: AFNOR, March 2013.

AFNOR. *Method of test for masonry. Part 1: Determination of compressive strength.* NF EN 1052-1. Paris, France: AFNOR, october 1999.

AFNOR. *Natural stone test method. Determination of real density and apparent density, and of total and open porosity.* NF EN 1936. Saint-Denis, France: AFNOR, may 2007.

AFNOR. *Natural stone test methods. Determination of static elastic modulus.* NF EN 14580. Saint-Denis, France: AFNOR, august 2005.

AFNOR. *Natural stone test methods. Determination of uniaxial compressive strength.* NF EN 1926. Saint-Denis, France: AFNOR, april 2007.

AFNOR. *Testing concrete in structures. Part 1: Cored specimens. Taking,examining and testing in compression.* NF EN 12504-1. Saint-Denis, France: AFNOR, April 2012.

AFNOR. *Testing hardened concrete. Part 1: Shape, dimensions and other requirements for specimens and moulds.* NF EN 12390-1. Saint-Denis, France: AFNOR, november 2012.

AFNOR. *Testing hardened concrete. Part 13: determination of secant modulus of elasticity in compression.* NF EN 12390-13. Saint-Denis, France: AFNOR, february 2014.

AFNOR. *Testing hardened concrete. Part 3: Compressive strenght of test specimens.* NF EN 12390-3. Saint-Denis, France: AFNOR, april 2012.

Backes, H.-P. "Tensile strength of masonry." Edited by Tom McNeilly and John C. Scrivener. *Proceedings of the 7th International Brick Masonry Conference.* Melbourne, Australia, 1985. 779-790.

Bazant, P., and B. H. Oh. "Crack band theory for fracture of concrete." *Materials and Structures*, no. 16 (1983): 155-177.

Bazant, Z.P., and P.A. Pfeiffer. "Shear fracture tests of concrete." *Materials and Structures* (Kluwer Academic Publishers) 19, no. 2 (1986b): 111-121.

Berto, Luisa, Anna Saetta, Roberto Scotta, and Renato Vitaliani. "An orthotropic damage model for masonry structures." *International Journal for Numerical Methods in Engineering* (John Wiley \& Sons, Ltd.) 55, no. 2 (2002): 127-157.

Biette, Louis. *Les chemins de fer urbains parisiens. Historique - Modalités de la construction de l'infrastructure.* Edited by J.-B. Baillière et fils. Vol. 1. J.-B. Baillière et fils, 1928.

Binda, L., A. Fontana, and G. Frigerio. "Mechanical behaviour of brick masoneries derived from unit and mortar characteristics." Edited by John W. de Courcy. *Proceedings 8th International Brick-Block. Masonry Conference.* Dublin, Ireland: Elsevier Applied Science, 1988.

Boulay, C., and A. Colson. "Un extensomètre à béton éliminant l'influence des déformations transversales sur la mesure des déformations longitudinales." *Matériaux et Construction* (Kluwer Academic Publishers) 14, no. 1 (1981): 35-38.

Chen, H-M, H-S Yu, and MJ Smith. "Physical model tests and numerical simulation for assessing the stability of brick-lined tunnels." *Tunnelling and Underground Space Technology* 53 (2016): 109-119.

Creazza, G., R. Matteazzi, A. Saetta, and R. Vitaliani. "Analyses of Masonry Vaults: A Macro Approach based on Three-Dimensional Damage Model." *Journal of Structural Engineering* 128, no. 5 (2002): 646-654.

Dhanasekar, M, AW Page, and PW Kleeman. "The failure of brick masonry under biaxial stresses." *Proceedings of the Institution of Civil Engineers* 79, no. 2 (1985): 295-313.

Domede, N., A. Sellier, and T. Stablon. "Structural analysis of a multi-span railway masonry bridge combining in situ observations, laboratory tests and damage modeling." *Engineering Structures* 56 (2013): 837-849.

Domède, N., G. Pons, A. Sellier, and Y. Fritih. "Mechanical behaviour of ancient masonry." *Materials and Structures* (Springer Netherlands) 42, no. 1 (2009): 123-133.

Drougkas, A., P. Roca, and C. Molins. "Material Characterization and Micro-Modeling of a Historic Brick Masonry Pillar." *International Journal of Architectural Heritage* 10, no. 7 (2016): 887-902.

Hillerborg, A., M. Modéer, and P.-E. Petersson. "Analysis of crack formation and crack growth in concrete by means of fracture mechanics and finite elements." *Cement and Concrete Research* 6, no. 6 (1976): 773-781.

Hillerborg, Arne. "Results of three comparative test series for determining the fracture energy GF of concrete." *Materials and Structures* (Kluwer Academic Publishers) 18, no. 5 (1985): 407-413.

Idris, J., Verdel.T, and M. Al-Heib. "Numerical modelling and mechanical behaviour analysis of ancient tunnel masonry structures." *Tunnelling and Underground Space Technology* 23 (2008): 251-263.

JSCE. *Shear strength test method for steel fiber reinforced concrete.* JSCE-G 553. Japan: JSCE, 1983, 1983.

Llanca, D., P. Breul, C. Bacconnet, and M. Sahli. "Characterization of the masonry lining of an underground structure by geoendoscopy." *Tunnelling and Underground Space Technology* 38 (2013): 254-265.

Lourenço, P.B., J.D. Rots, and R. van der Pluijm. "Understanding the tensile behaviour of masonry paralel to bed joints : a numerical approach." *Masonry International* 12, no. 3 (1999): 96-103.

McNary, W. Scott, and Daniel P. Abrams. "Mechanics of Masonry in Compression." *Journal of Structural Engineering* 111, no. 4 (1985): 857-870.

Mesnager, A. "Matériaux de Construction. Pierres." In *Encyclopédie du Génie Civil et des Travaux Publics*. Paris, France: J.-B. Baillière et fils, 1923.

Mirsayah, Amir A., and Nemkumar Banthia. "Shear Strength of Steel Fiber-Reinforced Concrete." *ACI Materials Journal* 99, no. 5 (2002): 473-479.

Moreno Regan, O, E Bourgeois, AS Colas, P Chatellier, A Desbordes, and JF Douroux. "Application of a coupled homogenization-damage model to masonry tunnel vaults." *Computers and Geotechnics* 83 (2017): 132-141.

Moreno Regan, Omar. "Study of the behavior of the masonry tunnels of the Paris subway system." Ph.D. dissertation (In French), Universté Paris-Es, Paris, France, 2016.

Page, AW. "The biaxial compressive strength of brick masonry." *Proceedings of the Institution of Civil Engineers* 71, no. 3 (1981): 893-906.

Pelà, L., Roca P., and A. Benedetti. "Mechanical Characterization of Historical Masonry by Core Drilling and Testing of Cylindrical Samples." *International Journal of Architectural Heritage* 10, no. 2-3 (2016): 360-374.

Rossi, Pierre, JanG.M. Van Mier, François Toutlemonde, and Fabrice Le Maou. "Effect of loading rate on the strength of concrete subjected to uniaxial tension." *Materials and Structures* (Kluwer Academic Publishers) 27, no. 5 (1994): 260-264.

Saade, Maamoun, Stephan Kesteloot, Chafika Djelal, Lotfi Hamitouche, and Idriss Benslimane. "Behavior of Millstone Masonry Vaults Strengthened by Composite Materials." *Journal of Civil Engineering and Architecture* 7, no. 8 (2013): 932-939.

Shah, S.P., S.E. Swartz, and C. Ouyang. *Fracture Mechanics of Concrete: Applications of Fracture Mechanics to Concrete, Rock and Other Quasi-Brittle Materials.* Wiley, 1995.

Vermeltfoort, A.Th., and T.M.J Raijmakers. "Deformation controlled tests in masonry shear walls. Part 2 (in dutch)." Eindhoven University of Technology, Eindhoven, The Netherlands, 1993.

Zucchini, A, and P.B Lourenço. "A coupled homogenisation-damage model for masonry cracking." *Computers and Structures* 82, no. 11-12 (2004): 917-929.

Figure list

Table list

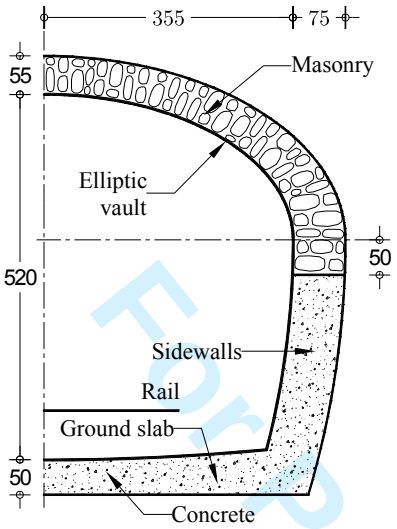

Fig. 1 Typical section of a tunnel of the Paris subway system and constitutive materials (in cm)

a) Compact sample b) Porous sample

Fig. 2. Samples of the stone (millstone/gritstone) used in the construction of the masonry vault

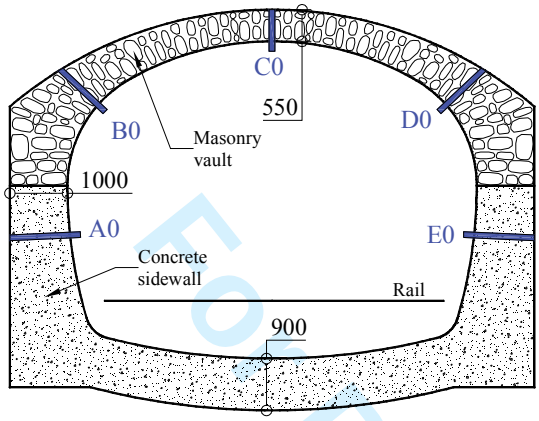

a) Chosen positions for the extraction of the cores (in mm)

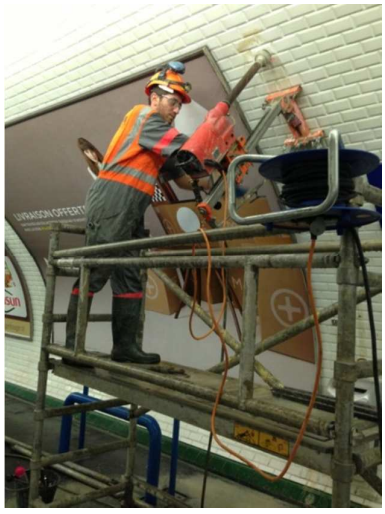

b) Extraction using a 76 mm core drilling sampler

Fig. 3. Core extraction

a) 50 mm diameter mortar specimen b) 104 mm diameter concrete specimen

Fig. 4. Size of the aggregates

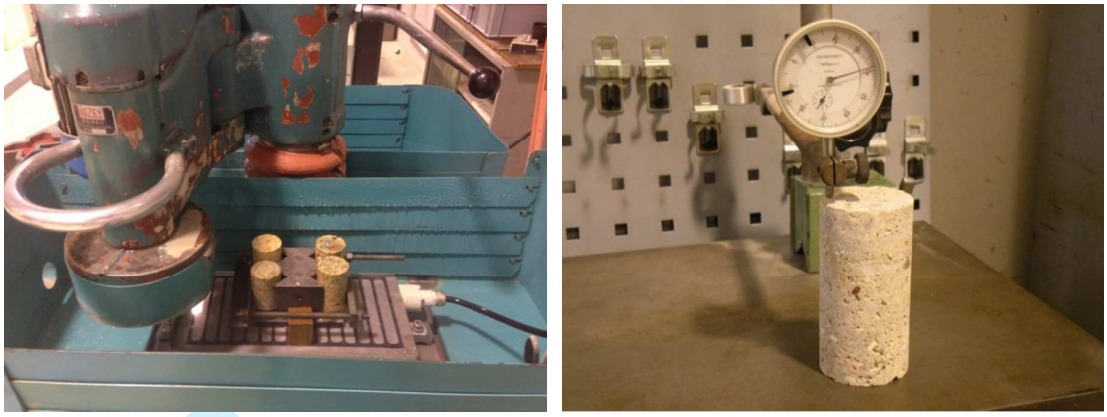

a) Mechanical surfacing b) Flatness check

Fig. 5. Preparation of the specimens

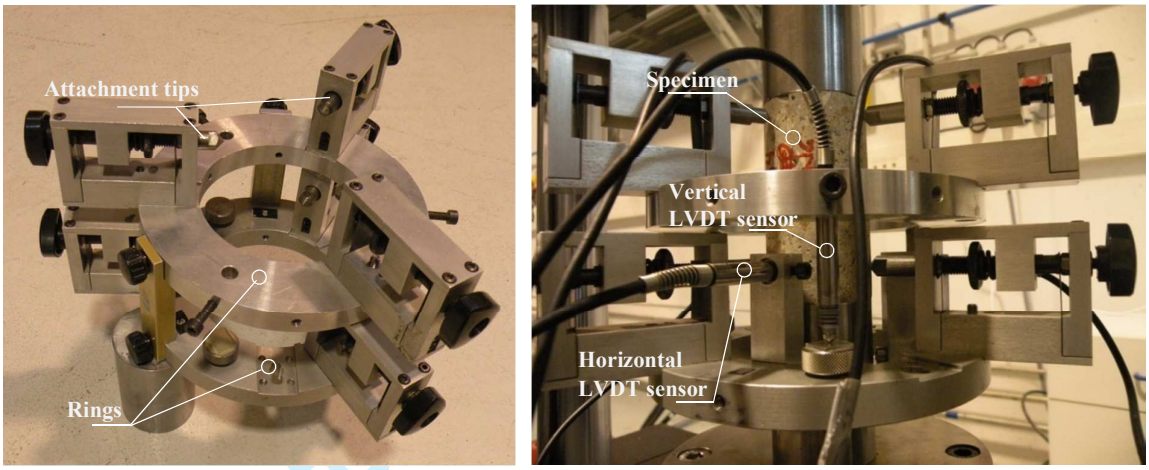

a) Device "J2P" (Boulay et Colson 1981) b) Device with sensors attached to the specimen

Fig. 6. Experimental measuring device for the compression tests

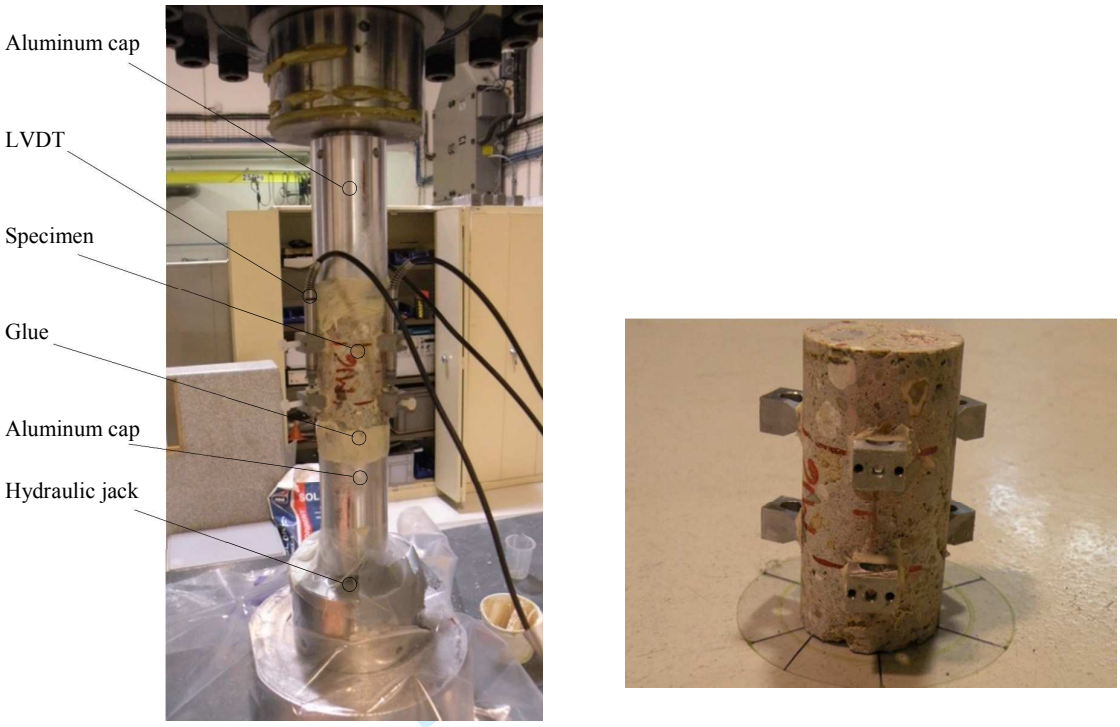

a) Glued specimen ready for the test

b) Supports of the LVDT sensors glued to the specimen

Fig. 7. Experimental device for the direct tensile tests

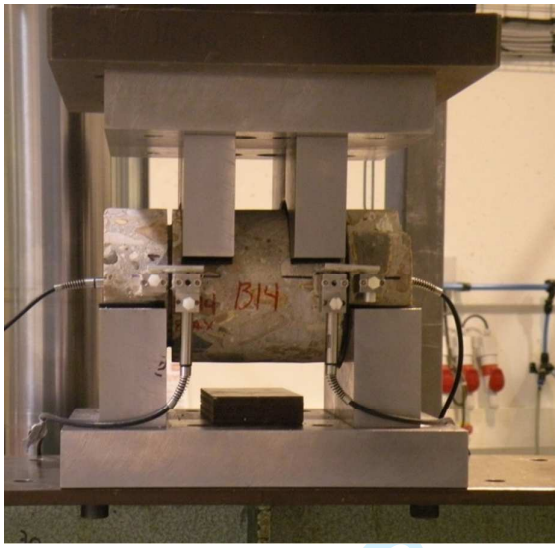

Fig. 8. Experimental device for the shear tests

Fig. 9. Mortar samples of 50 mm diameter

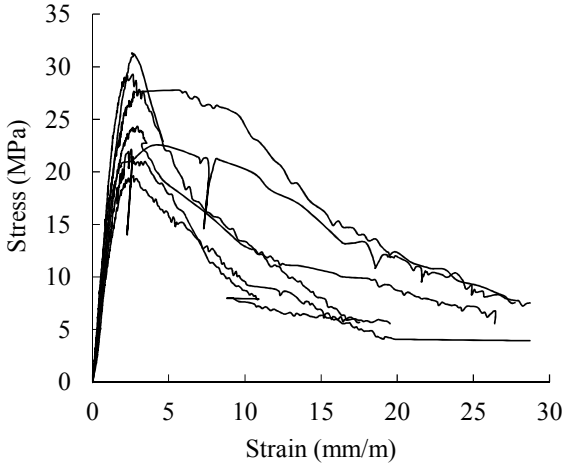

Fig. 10 Stress-strain curves the mortar compression tests from 7 specimens

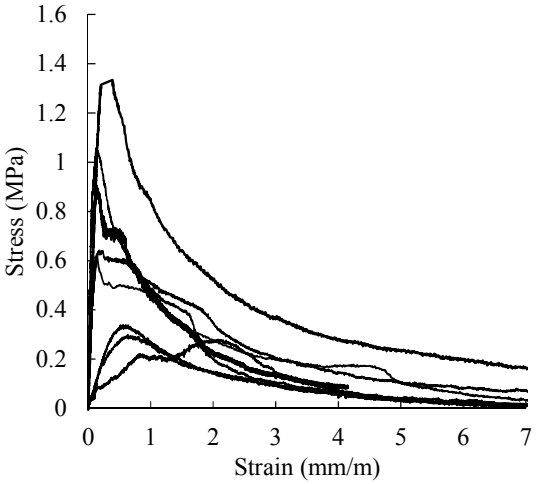

Fig. 11 Stress-strain curves for the mortar direct tensile tests from 8 specimens

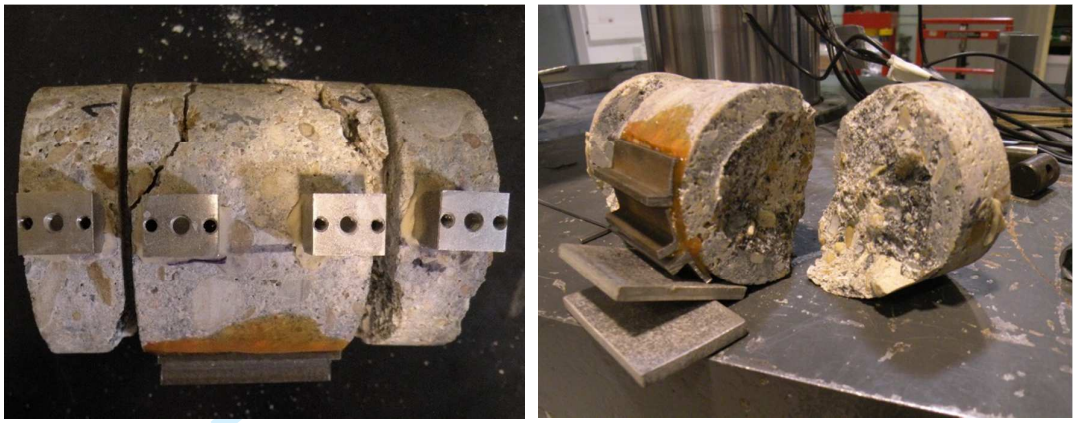

Fig. 12 Cracking of the mortar specimen in the shear test

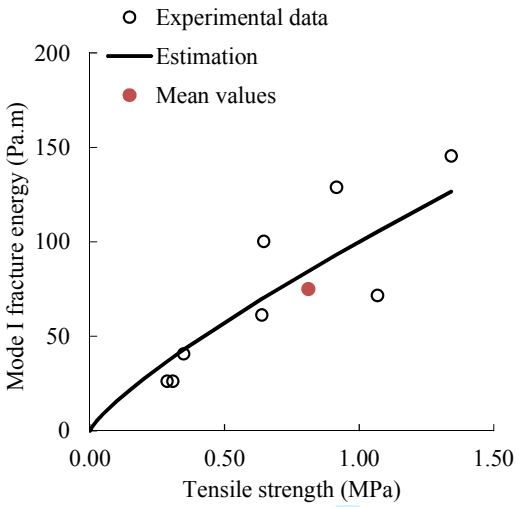

Fig. 13 Relation between tensile strength and mode I fracture energy for the mortar

High quality
$0\% < p_0 \leq 13\%$

Average quality
$13\% < p_0 \leq 35\%$

Low quality
$p_0 > 35\%$

Fig. 14 Observed composition of different types of Millstone and proposed classification regarding its porosity p_0

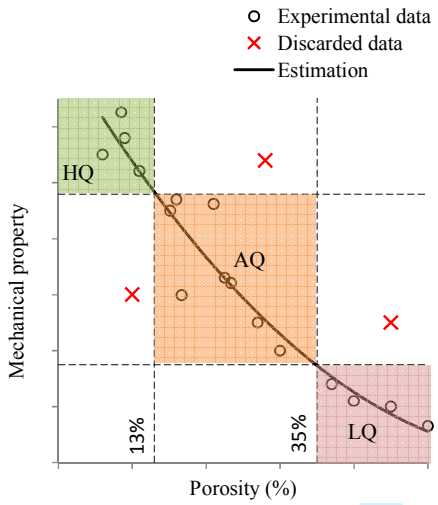

Fig. 15 Proposed ranges for the classification of the Millstone specimens (HQ: high quality; AV: average quality; LQ: low quality)

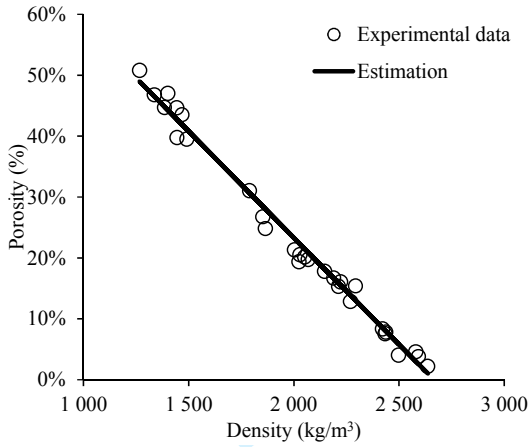

Fig. 16 Relation between porosity and density for the Millstone

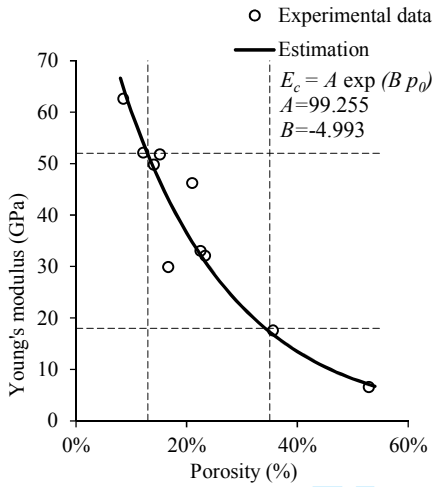

Fig. 17 Relation between Young's modulus and porosity for the Millstone from 10 specimens

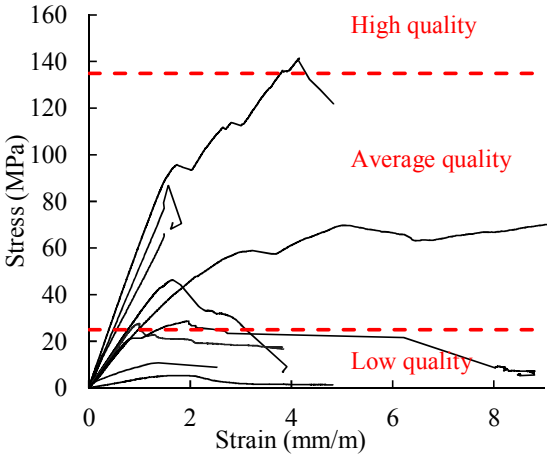

a) Stress-strain curves from 9 specimens of 50 mm diameter

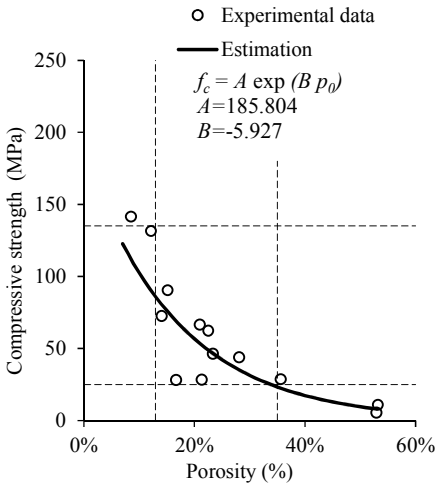

b) Relation between p_0 and f_c for 50 mm specimens

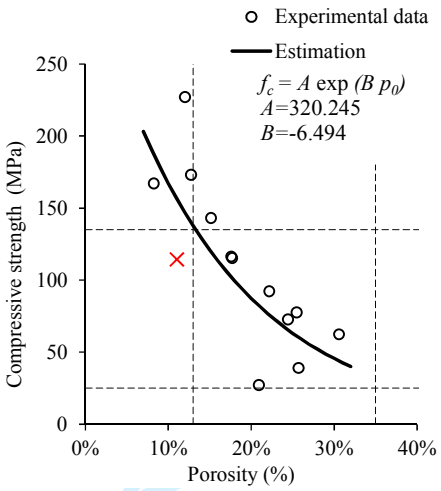

c) Relation between p_0 and f_c for 73 mm specimens

Fig. 18 Compression tests for the Millstone

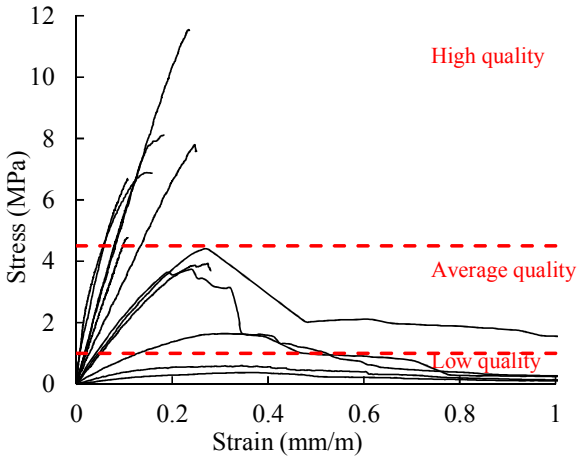

a) Stress-strain curves

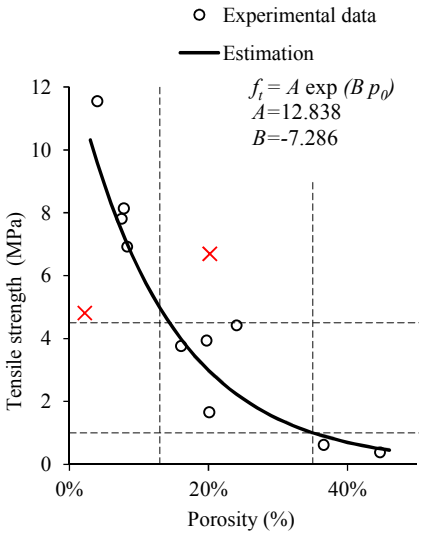

b) Relation between porosity and tensile strength

Fig. 19 Direct tensile tests from 12 Millstone specimens

Fig. 20. Concrete samples of 103 mm diameter

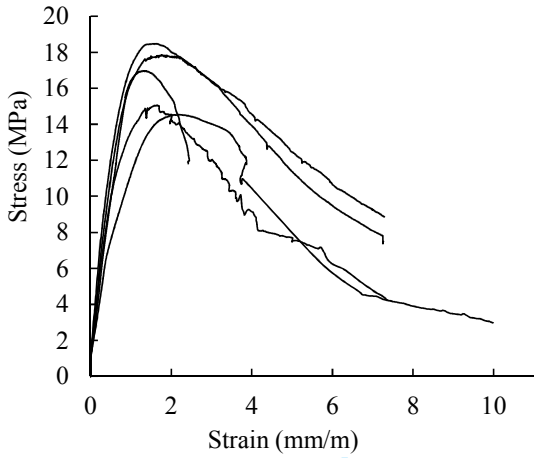

Fig. 21 Stress-strain curves for the concrete compression tests from 5 specimens

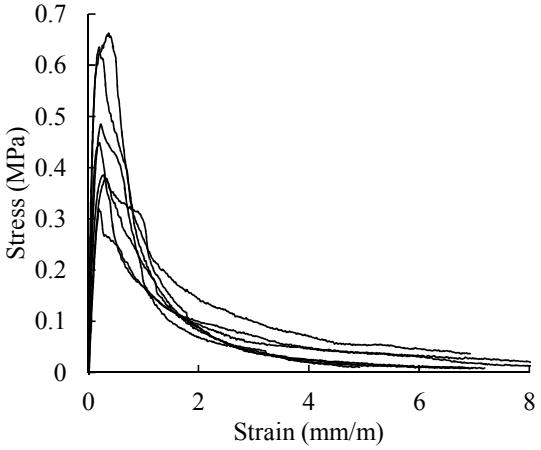

Fig. 22 Stress-strain curves for the concrete direct tensile tests from 7 specimens

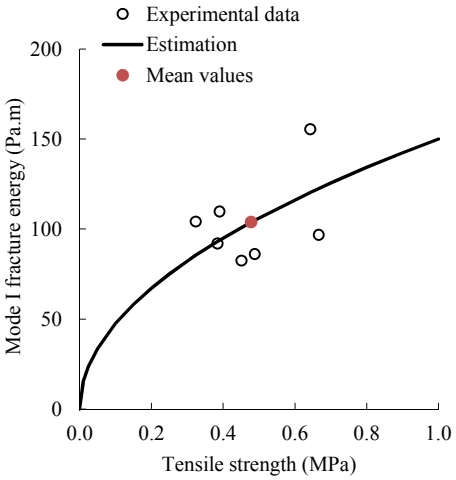

Fig. 23 Correlation between tensile strength and mode I fracture energy for the concrete

a) Samples

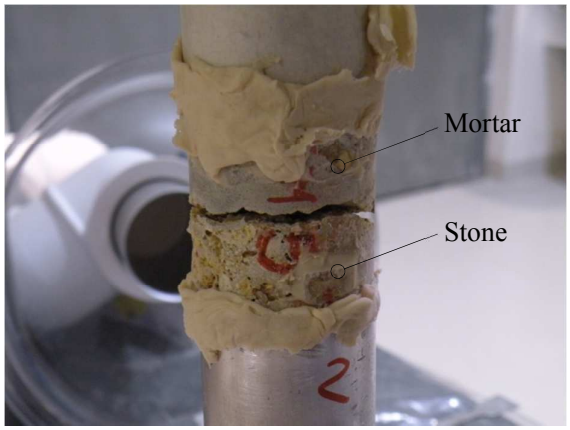

b) Crack at the stone-mortar interface

Fig. 24 Direct tensile tests on the masonry interface

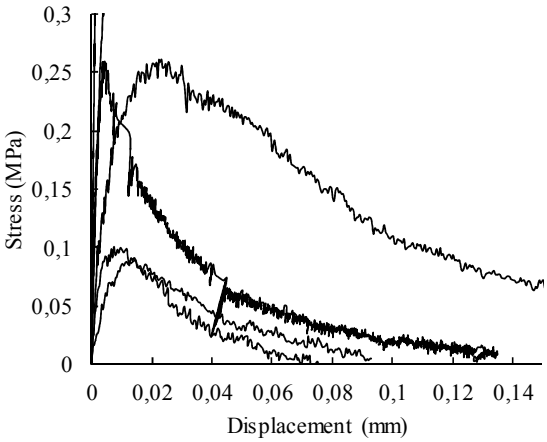

Fig. 25 Stress-displacement curves for the composite interface direct tensile tests from 6 specimens

Table 1 Description of the extracted cores

Ref.	Position	Number of cores	Diameter (mm)	Length (mm)	Material	Studied property				Sum
						E_c/f_c	f_t	f_s	ρ	
A0	Sidewalls	4	104	1100 – 2100	Concrete[1]	5	6	3	1	15
B0	Haunch	8	74	850 – 1300	Masonry[2]	15	10	2	18	45
C0	Keystone	8	74	500 – 700	Masonry[2]	7	11	4	9	31
D0	Haunch	8	74	850 – 1300	Masonry[2]	13	12	4	16	45
E0	Sidewalls	4	104	1100 – 2100	Concrete[1]	8	6	6	8	28
		32								**164**

[1]For some cores, masonry was also found in this part of the tunnel
[2]This includes the composite tests as well as the mortar and stone individual tests

Table 2 Test results for mortar specimens

Property		Retained samples	Mean	CV	Max	Min
Density (kg/m³)	ρ	9/9	2010	6%	2180	1 840
Porosity (%)	p_0	9/9	24%	18%	31%	17%
Compressive strength (MPa)	f_c	7/10	25.5	16%	36.6	19.9
Tensile strength (MPa)	f_t	11/12	0.81	47%	1.34	0.29
Shear strength (MPa)	f_s	4/6	1.42	12%	1.70	1.25
Elastic modulus (GPa)	E_c	4/5	19.4	6%	20.8	17.6
Poisson's ratio	ν	5/5	0.15	22%	0.20	0.11
Mode I fracture energy (Pa.m)	G_{fI}	8/9	75.0	57%	145	26
Mode II fracture energy (Pa.m)	G_{fs}	-	148	-	-	-

Table 3 Test results for stone specimens

Property		High quality					Average quality					Low quality				
		Retained samples	Mean	CV	Max	Min	Retained samples	Mean	CV	Max	Min	Retained samples	Mean	CV	Max	Min
Density (kg/m³)	ρ	8/29	2490	4%	2640	2 270	13/29	2060	7%	2300	1 800	8/29	1410	5%	1500	1 270
Porosity (%)	p_0	8/29	6%	50%	13%	2%	13/29	20%	22%	31%	15%	8/29	45%	8%	51%	39%
Compressive strength (MPa)[1]	f_c	4/13	178	17%	227	143	8/13	75.3	40%	116	27.0	-	-	-	-	-
Compressive strength (MPa)[2]	f_c	2/13	137	4%	142	132	8/13	54.7	38%	90.3	28.1	3/13	15.0	66%	28.7	5.4
Tensile strength (MPa)	f_t	4/12	8.60	20%	11.5	6.91	4/12	3.44	31%	4.42	1.65	2/12	0.50	24%	0.62	0.38
Shear strength (MPa)	f_s	-	-	-	-	-	5/6	4.83	22%	6.4	3.55	-	-	-	-	-
Elastic modulus (GPa)	E_c	2/10	57.4	9%	62.6	52.1	6/10	40.5	22%	51.8	51.8	2/10	12.1	45%	17.6	6.6
Poisson's ratio	ν	2/10	0.18	4%	0.19	0.17	4/10	0.32	23%	0.41	0.22	-	-	-	-	-
Mode I fracture energy (Pa.m)	G_{fI}	3/12	6.68	52%	11.0	2.48	2/12	121	21%	146	95	2/12	28	8%	30	26

[1]Specimens of 73 mm diameter

[2]Specimens of 50 mm diameter

Table 4 Test results for masonry specimens

Masonry property		Retained samples	Mean	CV	Max	Min
Density (kg/m³)	ρ	8/8	2030	11%	2390	1 730
Porosity (%)	p_0	8/8	22%	38%	34%	8%
Compressive strength (MPa)	f_c	5/5	21.7	68%	49.7	9.8
Elastic modulus (GPa)	E_c	5/5	28.4	61%	59.5	10.5
Interface property						
Tensile strength (MPa)	f_t	11/13	0.15	56%	0.27	0.04
Mode I fracture energy (Pa.m)	G_{fI}	6/8	8.30	88%	23.2	1.54
Normal stiffness (GPa/m)	k_n	8/8	64.8	95%	176	2.62

Table 5 Test results for concrete specimens

Property		Retained samples	Mean	CV	Max	Min
Density (kg/m³)	ρ	5/6	2160	1%	2180	2 130
Porosity (%)	p_0	5/6	18%	4%	19%	17%
Compressive strength (MPa)	f_c	6/7	16.0	13%	18.5	12.6
Tensile strength (MPa)	f_t	7/8	0.48	25%	0.67	0.32
Shear strength (MPa)	f_s	6/7	0.89	16%	1.10	0.71
Elastic modulus (GPa)	E_c	7/7	21.9	19%	27.6	16.4
Poisson's ratio	ν	7/7	0.21	11%	0.26	0.18
Mode I fracture energy (Pa.m)	G_{fI}	7/8	104	22%	155	82